

Enzymatic Janus Liposome Micromotors

Hui Jin, Jinyan Cui, and Wei Zhan*

Cite This: *Langmuir* 2023, 39, 4198–4206

Read Online

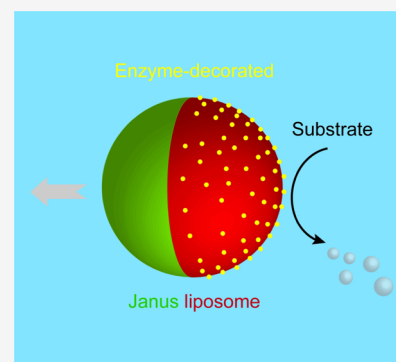
ACCESS |

Metrics & More

Article Recommendations

Supporting Information

ABSTRACT: A liposome-based micromotor system that utilizes regional enzymatic conversion and gas generation to achieve directional motion in water is presented. Constituted mainly of a low-melting lipid and a high-melting lipid together with cholesterol, these liposomes maintain stable Janus configuration at room temperature as a result of lipid liquid–liquid phase separation. Local placement of enzymes such as horseradish peroxidase is realized via affinity binding between avidin and biotin, the latter as a lipid conjugate sorted specifically into one domain of these Janus liposomes as a minor component. In the presence of the substrate, hydrogen peroxide, these enzyme-decorated Janus liposomes undergo directional motion, yielding velocities exceeding thermal diffusion by three folds in some cases. Experimental details on liposome size control, motor assembly, and substrate distribution are presented; effects of key experimental factors on liposome motion, such as substrate concentration and liposome Janus ratio, are also examined. This work thus provides a viable approach to building asymmetrical lipid-assembled, enzyme-attached colloids and, in addition, stresses the importance of asymmetry in achieving particle directional motion.



INTRODUCTION

Artificial nano-/micromotors have attracted much research interest in recent years owing to their promise for advanced materials with built-in motility. Sophisticated functionality and exotic collective behavior, ranging from on-demand drug delivery, nanorobotics to active matter, have been envisioned.^{1–4} As a class of water-dispersed, intrinsically biocompatible colloidal assemblies, liposomes have established diverse and widespread utility in both basic research (e.g., membrane biophysics,⁵ protocells,⁶ and lubrication⁷) and commercial (e.g., drug delivery,⁸ food,⁹ cosmetics,¹⁰ and immunoassays¹¹) avenues; exploring their physicochemical characteristics and performance as artificial motors, therefore, bears significant fundamental as well as practical implications. Herein, we present a liposome-based micromotor system in which directional particle motion is realized through regionally executed enzymatic gas production. To the existing body of work exploiting liposomes or gas-generating enzymes to build nano-/micromotors, this work thus adds a new example in which localized enzyme activity is furnished out through asymmetrical liposome carriers.

Combining high efficiency/specificity of one with the broken symmetry of the other, enzyme-coated Janus particles provide an attractive approach to artificial motors. Among numerous enzymatic systems^{12–16} being investigated, catalase and urease stand out for their effective gas (O_2 or CO_2) production from naturally occurring, small-molecule substrates (H_2O_2 or urea), conveniently affording design schemes for gas-propelled artificial motors navigating in aqueous media. As for enzyme on-particle placement, conventional bioimmobilization methods (e.g., covalent conjugation and physical adsorption)

coupled with various masking schemes have yielded reliable and precise modification of individual inorganic/polymer nanoparticles.^{17–20} Performance wise, these enzyme-attached Janus particles typically display enhanced diffusion^{15,16} in the presence of enzymatic substrates—a result of fast rotational diffusion randomizing their directional motion at this length scale.^{21,22} Besides size and broken symmetry of Janus particles, other enzyme-associated properties, such as their loading, catalytic efficiency, and stability, have also been shown to impact the mobility of these enzyme-powered motors.^{12,23} How to maintain enzyme activity during the operation of these artificial motors, in particular, is considered as one of the major issues currently impeding their routine biomedical applications.^{1,13,14}

With their minuscule, spherically sealed lipid bilayer(s) fully immersed in water on both sides, liposomes represent versatile colloidal carriers of biomolecules:^{24–26} depending on their size/polarity, the latter may be anchored either within the lipid bilayer or on liposome surface, or encapsulated inside the aqueous core of liposomes. Recognizing these attractive features, Cremer, Velegol, Sen, and their co-workers recently investigated microscopic movement of several enzyme-carrying liposome systems.^{27,28} Under parallel laminar flow conditions, nanosized liposomes coated with catalase and urease were

Received: February 3, 2023

Revised: February 28, 2023

Published: March 9, 2023



found to undergo positive and negative chemotaxis,²⁷ respectively, when subjected to their substrate; in solution, liposomes embedded with ATPase were observed to perform enhanced diffusion in the presence of ATP.²⁸ Taking further advantage of liposome's encapsulation capability, Patiño, Maspocho, Sánchez, and their co-workers developed liposome nanomotors with urease either coated on surface of or encapsulated within liposomes.²⁹ While the intact urease-encapsulated liposomes display no active motion with urea present outside, disrupting the liposome bilayer, combined with acidic treatments, led to a nearly one-fold mobility increase compared to background diffusion. These results clearly demonstrated the usefulness of liposomes in building enzyme-powered artificial motors. While no literature precedents exist in which Janus liposomes are employed in tandem with enzymatic gas generation to achieve active motion, the potential benefits of such coupling have been clearly demonstrated through their synthetic cousins, polymerosomes.^{30,31}

In this work, we present a proof-of-concept example of Janus liposome-based, enzyme-powered artificial motor systems. Horseradish peroxidase (HRP), a gas-generating enzyme, is selectively placed on phase-separated Janus liposomes, using domain-specific sorting of biotinylated lipids followed by enzyme conjugation via avidin/biotin binding. In the presence of HRP's substrate, H_2O_2 , these HRP-decorated Janus liposomes undergo directional motion, yielding velocities up to 3 times greater than their thermal diffusion. By contrast, such enhanced mobility is absent from homogeneous enzyme-decorated liposomes subjected to similar treatments. Motional characteristics of these enzyme-attached Janus liposome motors are compared with an enzyme-free liposome active motion system³² we reported recently. Effects of other key experimental factors on liposome motion, including substrate distribution/concentration and liposome Janus ratio, are also examined in detail.

RESULTS AND DISCUSSION

Liposome Motor Design. A schematic drawing of essential components of our enzymatic liposome motors is shown in Figure 1. Composition wise, these liposomes contain mainly three lipids, DOPC/DPPC/cholesterol, in a 35:35:30

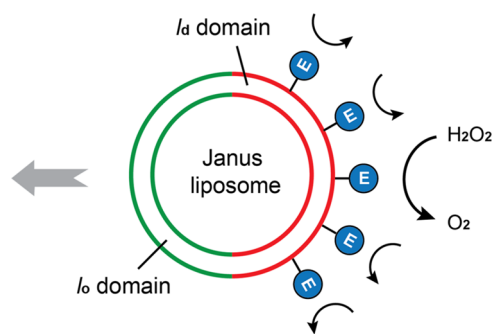


Figure 1. Design of enzymatic Janus liposome micromotors. The double circles indicate the lipid bilayer of the liposome, whereas its Janus configuration is denoted by green/red colors. Enzymes (E), such as horseradish hydrogen peroxidase (HRP) investigated here, are conjugated to the outer surface of the l_d domain of Janus liposomes via biotin/avidin binding. The substrate of HRP, hydrogen peroxide (H_2O_2), is present both inside and outside Janus liposomes during their movement.

mole ratio, which together yield a liquid-disordered (l_d) lipid domain phase-separated from a liquid-ordered (l_o) half within individual liposomes at room temperature, i.e., Janus liposomes.³³ These liposomes are additionally doped with three minor components: fluorescent $l_d(l_o)$ phase indicator; rhodope (Bodipy-Chol), both at 0.2%; and biotin-DOPE typically held at 1%. The latter is employed to anchor enzymes on the liposome surface through biotin/avidin binding. Importantly, since biotin-DOPE can be prepared to reside in the l_d domain nearly exclusively (see below), the enzyme to be anchored, HRP, will only decorate the outer surface associated with the l_d hemisphere of a liposome upon affinity binding. In the presence of their substrate (H_2O_2), accordingly, these regionally arranged enzymes will generate oxygen primarily near the l_d hemisphere of the host liposome, propelling the latter forward.

Liposome Motor Assembly and Characterization. It thus takes two steps to construct such liposome motors: (1) sorting biotin-DOPE into the l_d -domain of Janus liposomes, followed by (2) enzyme attachment thereabout via biotin/avidin binding. To maximize gas production, one generally prefers high biotin-DOPE loading in liposomes (step 1), which, however, could disrupt the lipid organization/phase equilibrium preestablished by DOPC/DPPC/Chol if unchecked. Similarly, the subsequent biotin/avidin-HRP binding (step 2) may introduce additional perturbation to liposomes due to the multivalent nature of such binding.

To identify optimal assembling conditions, we examined l_d -labeled Janus liposomes subjected to a series of biotin-DOPE doping levels and avidin mixing ratios. As shown in Figure 2, biotin-DOPE at 1 mol% doping level remains largely l_d -associated in Janus liposomes, consistent with our previous observation.³³ Assuming an even split between l_d and l_o domains, such exclusive association of biotin-DOPE doubles its effective concentration in the l_d domain to 2%. When such biotinylated Janus liposomes were incubated externally with avidin at 5:1 (with biotin in excess to minimize free avidin in solution) mixing ratio; moreover, a fairly even coat of avidin on the l_d -hemisphere was obtained (Figure 2c). Higher mixing ratios, for example, 5:1.5 or 5:2, were found to yield denser avidin layers under similar incubation conditions, which, however, were accompanied frequently by liposome morphology changes (e.g., disrupted domains and dotted formations on liposome surfaces) as well as liposome aggregation (Figure S1). By contrast, such unfavorable liposome modifications were minimal at the 5:1 biotin-to-avidin binding ratio. To ensure good enzyme coverage while maintaining the integrity/entirety of individual Janus liposomes, we thus chose 1% biotin-DOPE 5:1 bound to avidin-HRP to build our liposome motors.

Liposome Size Control. To be able to quantitatively assess liposome active motion resulted from enzymatic gas production, the passive component of liposome movement, i.e., thermal diffusion, must also be accounted for. According to Stokes–Einstein equation, $D = kT/6\pi\eta r$, where kT is the thermal energy, η is the viscosity of the medium, and r is the radius of the particle, the extent of diffusion of a spherical particle scales inversely proportionally to its size. To keep liposome diffusion at a relatively constant level, we thus sought to control their size using membrane extrusion (Experimental Section). As shown in Figure 3, liposome samples as prepared display a wide range of sizes, which, upon extrusion through 5- μ m-diameter porous membranes, can be effectively narrowed

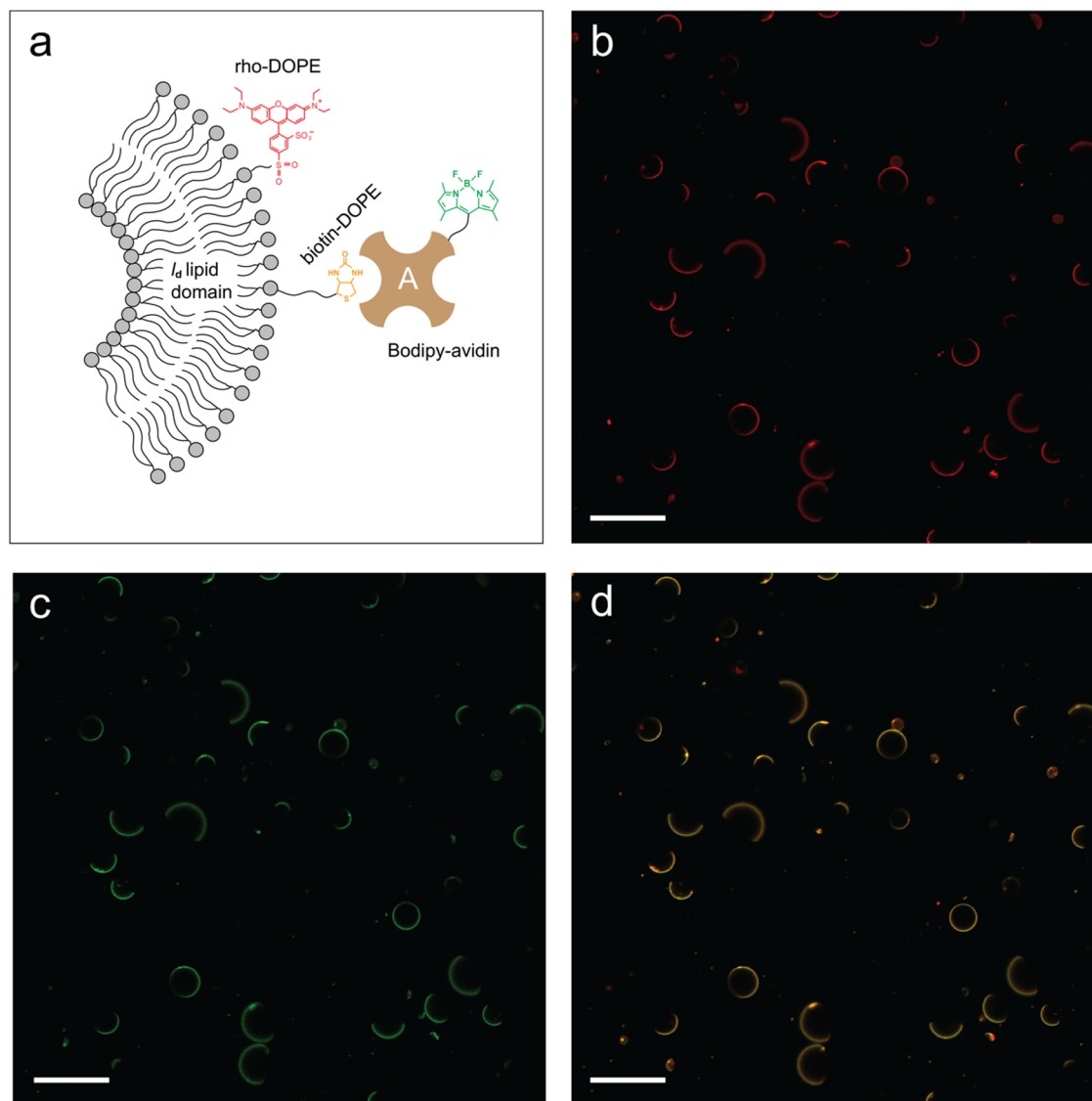


Figure 2. Fluorescence microscopic characterization of biotin-DOPE localization in DPPC/DOPC/cholesterol Janus liposomes. (a) Cartoon depiction of fluorescently monitoring liposome l_d domain (shown in part) with rho-DOPE and biotin-DOPE via Bodipy-labeled avidin. (b) Red-channel (rho-DOPE) fluorescence micrograph revealing the l_d -domain of Janus liposomes; lipid composition: DPPC/DOPC/Chol (35:35:30 in mole ratio) containing additionally 0.2% rho-DOPE. (c) Green fluorescence image showing avidin location of the same liposome sample. The level of avidin is controlled to be roughly 1:5 relative to available biotin-DOPE (see the [Experimental Section](#)). (d) Merged fluorescence image of (b) and (c). Scale bar: 50 μm .

down to be around 5 μm . For Janus liposomes, importantly, the Janus configuration in the end product appears to be relatively unaffected after such hydraulic treatment. It is possible to prepare smaller liposomes by extrusion employing membranes with finer pores, which, however, makes it challenging to reliably discern the two domains in Janus liposomes.

Substrate (H_2O_2) Distribution in the System. With all lipid constituents dynamically assembled into a bilayer-enclosed architecture, liposomes differ fundamentally from their inorganic/polymer counterparts for building motors. Their structural thinness and softness, first and foremost, directly impact their mechanical stability and hence the integrity of resultant motors. This is especially the case for micro-sized liposomes studied here, in which microscopic membrane deformation is largely decoupled with nanoscopic bending from individual lipids and thus respond freely to

surface tension and other environmental agitations.^{34–36} If, for example, a species with limited permeability to the liposome bilayer is only present on one side of the liposome, a concentration gradient would result across the bilayer. This, in turn, will produce an osmotic pressure that can be too great for the liposome to withstand—a detrimental outcome for its intended application.

To determine whether H_2O_2 poses any osmotic shock to liposomes investigated here, we next monitored liposome samples subjected to a sudden H_2O_2 concentration jump in the surroundings. As shown in [Figure 4](#), Janus liposomes upon exposure to ~ 80 mM (or 0.8 wt%) H_2O_2 were able to maintain not only their phase-separated morphology but, to a great extent, also their size. Similar observations were also obtained at higher H_2O_2 concentrations (up to 5 wt%) as well as from homogeneous DOPC liposomes (data not shown). These results thus suggest that H_2O_2 readily permeates and

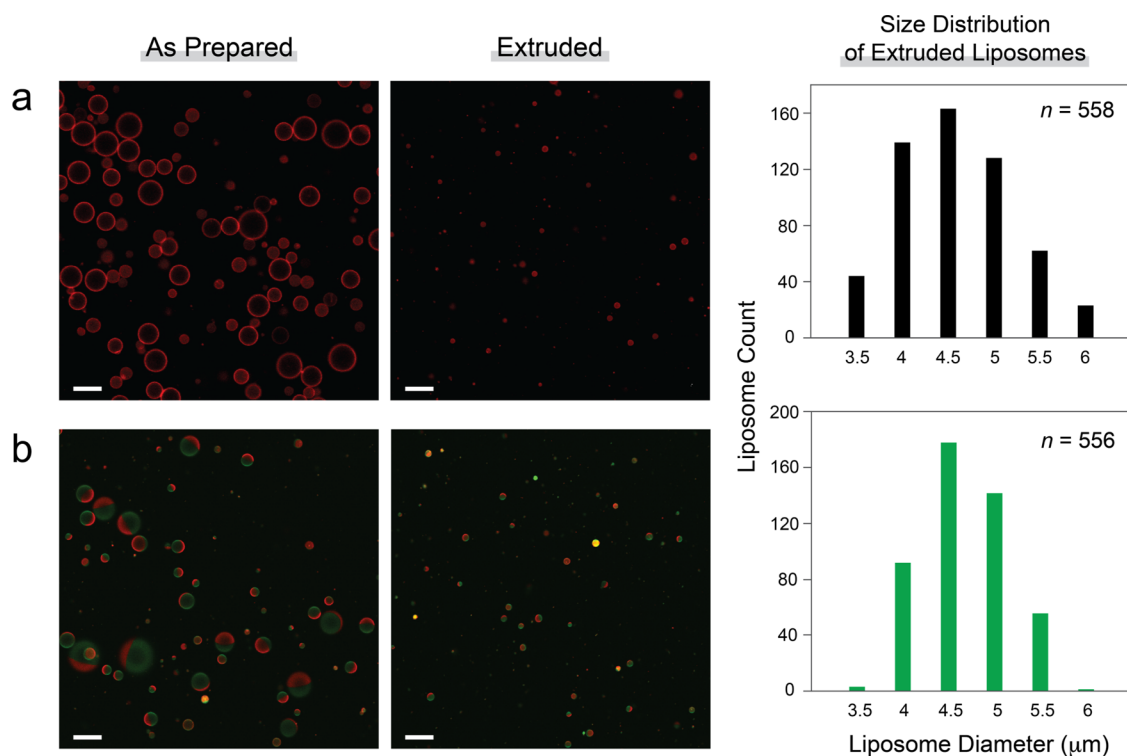


Figure 3. Fluorescence images of liposomes before/after size control via extrusion and their size distribution. (a) Homogeneous DOPC/Chol (70/30, mole ratio) liposomes doped in addition with 0.2% rho-DOPE ($n = 558$). (b) DPPC/DOPC/Chol (35/35/30) Janus liposomes containing also 0.2% Bodipy-Chol and rho-DOPE each ($n = 556$). Liposome counts are reported in 0.5- μm size groups with their lower size limits identified in the histograms. Scale bar: 25 μm .

equilibrates across DOPC/DPPC/Chol bilayers, at least on the second (s) timescale if not much faster.³⁷ Permeability coefficients of H_2O_2 across l_d and l_o lipid bilayers became available just recently, with the former measured to be at 1×10^{-3} cm/s level for DOPC/POPG/Chol liposomes.³⁸ For reference, this value is roughly an order of magnitude greater than water permeation across Chol-mixed lipid membranes,³⁹ whereas oxygen, the product of H_2O_2 enzymatic breakdown, permeates much more readily (on the order of 1×10^2 cm/s).⁴⁰

Also included in Figure 4 are control measurements of Janus liposomes similarly treated with sucrose instead. Owing to its high water solubility and low lipid permeability, sucrose is frequently employed as an osmolyte to enforce osmotic imbalance across lipid membranes.⁴¹ Its hydrogen-bonding capability and high density (relative to water alone), in addition, are quite useful in liposome preparation and sedimentation.^{24,42} According to van't Hoff equation, $\Delta\Pi = \Delta c kT$, where Δc is the concentration gradient and $\Delta\Pi$ is the resultant osmotic pressure, 24 mM sucrose introduced externally would exert an osmotic pressure of nearly 60 kPa across the liposome bilayers. The resulting force, in turn, squeezes and crushes the liposome all around, quickly shrinking the latter into a much smaller particle with crumpled and intermixed lipid domains (Figure 4b).

Enzymatic Gas-Driven Motion of Janus Liposomes. With background diffusion properly controlled and substrate distribution in the system known, we next investigated liposome movement trajectories and speed under various conditions. In each case, we perform mean-square displacement (MSD) analysis on >500 liposome trajectories to obtain a robust, ensemble-averaged displacement plot (Experimental

Section). As shown in Figure 5a, HRP- l_d -attached Janus liposomes in the presence of H_2O_2 collectively yield an upward-bending MSD plot, indicative of the presence of active motion component in the system that is superimposed with background diffusion. When either the enzyme or its substrate is taken out of the system, in contrast, only sublinear MSD plots characteristic of diffusion-dominant motion^{21,22} were obtained (Figure 5b,c). These negative controls thus point to enzymatic gas production as the driving force of liposome active motion. Furthermore, when homogeneous DOPC liposomes were used as motor construct in place of Janus liposomes (while keeping both HRP and H_2O_2 in the system), only background-level displacements were observed (Figure 5d). This result stresses once again the importance of particle asymmetry in achieving liposome active motion:³² interfacial reactivity (i.e., gas generation), a necessary condition for particle propulsion, can fall insufficient if it gets canceled out around the particle due to the latter's spherical symmetry.

Fitting the ensemble-averaged MSD plot in Figure 5a into the diffusion-with-flow model,^{21,43} $\text{MSD}(t) = v_0^2 t^2 + 4Dt$, we then obtained the active motion velocity (v_0) and translational diffusivity (D), $2.7 \times 10^{-1} \mu\text{m s}^{-1}$ and $8.6 \times 10^{-2} \mu\text{m}^2 \text{s}^{-1}$, of the system being tested. Treating the three negative controls as diffusion-only cases, we in turn estimated their diffusivity: $8.7 \times 10^{-2} \mu\text{m}^2 \text{s}^{-1}$ (substrate-free), $9.4 \times 10^{-2} \mu\text{m}^2 \text{s}^{-1}$ (enzyme-free), $9.7 \times 10^{-2} \mu\text{m}^2 \text{s}^{-1}$ (homogeneous liposomes), respectively, following $\text{MSD}(t) = 4Dt$. These MSD-derived diffusivity values are in general agreement with that predicted ($1.0 \times 10^{-1} \mu\text{m}^2 \text{s}^{-1}$) by the Stokes–Einstein equation for spherical particles of 4.5- μm diameter. Using the same liposome size, we further obtained Péclet number (Pe)²¹ of 14.1 associated with the active case, from $\text{Pe} = 2rv_0/D$, which

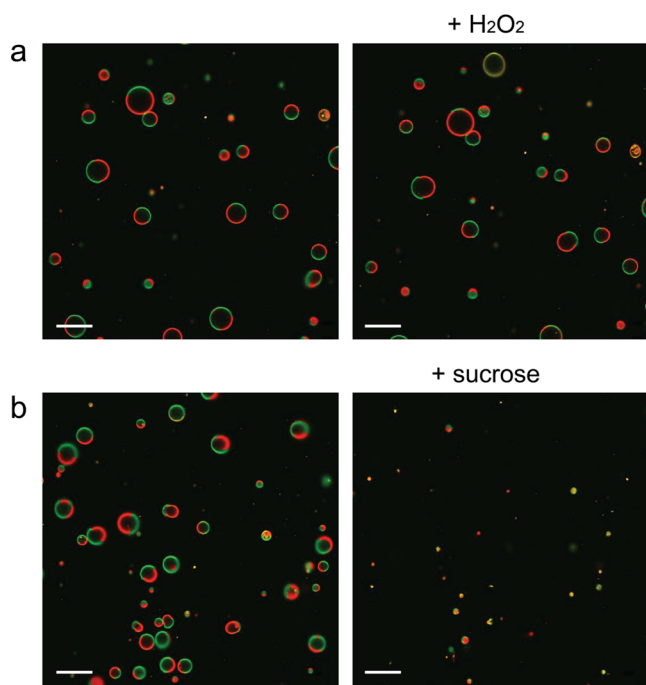


Figure 4. Fast permeation/equilibration of H_2O_2 across the lipid bilayer of Janus liposomes. (a) Fluorescence snapshots of Janus liposomes before/after being treated with H_2O_2 . The effective H_2O_2 concentration upon homogenization is ~ 80 mM. (b) Fluorescence snapshots of Janus liposomes samples before/after being similarly treated with ~ 24 mM sucrose. Same liposome sample (DPPC/DOPC/Chol, 35:35:30, with 0.2% Bodipy-Chol and rho-DOPE) was employed; in both cases, the two frames are taken a few seconds apart. Scale bar: $50 \mu\text{m}$.

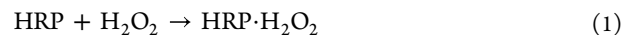
denotes the magnitude of active motion component relative to diffusion.

Different levels of liposome movement among these samples are also evident from examining representative trajectories of individual liposomes (Figure 6). While particles in control groups typically display clustered trajectories featuring short stepwise displacements over the 15-s monitoring window, liposomes undergoing active motion tend to produce more extended traces. A closer examination further reveals that the majority of these active liposomes (45%) move in a directional fashion, in that the particle tends to move along the direction defined by the initial orientation of its l_d (rear) and l_o (front) domains (Figure 6d). Due to thermal randomization and liposome rotational motion, trajectories that display overall sideways as well as backward movement were also found, which occur at lower frequencies. Fluorescence videos of Janus liposome movement under enzymatic conversion as well as control conditions are included in the Supporting Information (Videos S1–S4).

Effect of H_2O_2 Concentration on Liposome Active Motion. Since liposome active motion is propelled by enzymatic gas generation, the extent of which is directly proportional to the substrate concentration, we next examined movement of HRP-coated Janus liposomes under different H_2O_2 concentrations. As shown in Figure 7, a small enhancement in liposome motion became appreciable in the presence of 0.01 wt % H_2O_2 . As the concentration increases, the resultant MSD plots tick upward accordingly. The extent of increase, however, appears to slow down toward higher

concentrations (3–5% H_2O_2), which may be due to substrate saturation.

In terms of enzymatic action, HRP first binds H_2O_2 with 1:1 stoichiometry to produce a highly oxidizing precursor, which, upon encountering and oxidizing 2 equiv of a reductant (2AH_2), regenerates the enzyme together with water as a coproduct as follows.⁴⁴



In this sequence, therefore, H_2O_2 acts as an oxidant. When no reductant substrates are present in the system, alternatively, H_2O_2 will fill in as the reductant in the second step^{45,46}



In this case, therefore, HRP behaves analogously to catalase, converting H_2O_2 to release oxygen and water. It is thus this alternative pathway by which our liposome motor operates. Kinetically, the initial HRP/ H_2O_2 binding proceeds quite facilely ($k = 2 \times 10^7 \text{ M}^{-1} \text{ s}^{-1}$), whereas an apparent rate constant of $\sim 1.8 \text{ s}^{-1}$ was determined directly from oxygen production for the catalase-like pathway.⁴⁵ In these steady-state, solution-based measurements, the speed of oxygen production was found to increase with higher H_2O_2 concentrations, reaching saturation at about 40 mM.⁴⁶ Physiologically, this pathway has been proposed as a defense mechanism for plants in response to H_2O_2 burst during pathogenic attack.

Effect of Janus Ratio on the Activity of Janus Liposome Micromotors. A unique feature associated with phase-separated Janus liposomes is their tunable l_d -to- l_o area ratio, i.e., Janus ratio, which is accessible through control of lipid composition as long as it operates within the liquid–liquid coexistence region defined by the lipid phase diagram.³³ Previously, we have shown that the Janus ratio of DOPC/DPPC/Chol Janus liposomes can be tuned by nearly an order of magnitude by adjusting the mixing ratio of the three components.³³ Since the relative size of l_d domain directly defines the active, enzyme-coated portion of Janus liposomes, we next examined whether different Janus ratios directly impact the mobility of resultant motors.

As shown in Figure S2, MSD plots obtained from l_d -major (DOPC/DPPC/Chol: 50/30/20; Janus ratio: $\sim 3:1$) and l_d -minor (20/50/30; $\sim 1:3$) Janus liposomes appear closely comparable, both slightly less active than domain-even-split samples (35/35/30). Such closeness in particle displacement may result from the same doping level (1 mol %) of biotin-DOPE in all three samples, which would accommodate same load of enzymes but with different surface densities. Assuming comparable gas production per particle among the three samples, furthermore, geometry considerations favor liposome motors with a 1:1 Janus ratio: While propulsion only exerts on a small portion of the particle in l_d -minor liposomes, gas production past the liposome equator, as the case for l_d -major samples, can lead to partial cancellation of propulsion. Taking the latter scenario to the extreme case—homogeneous DOPC/Chol liposomes without broken surface symmetry—such cancellation would then become total (Figure Sd). In line with the observed results, this interpretation should be taken with caution, however. Several other complicating factors, such as variations in liposome size, Janus ratio (within the same population) as well as secondary modifications caused by

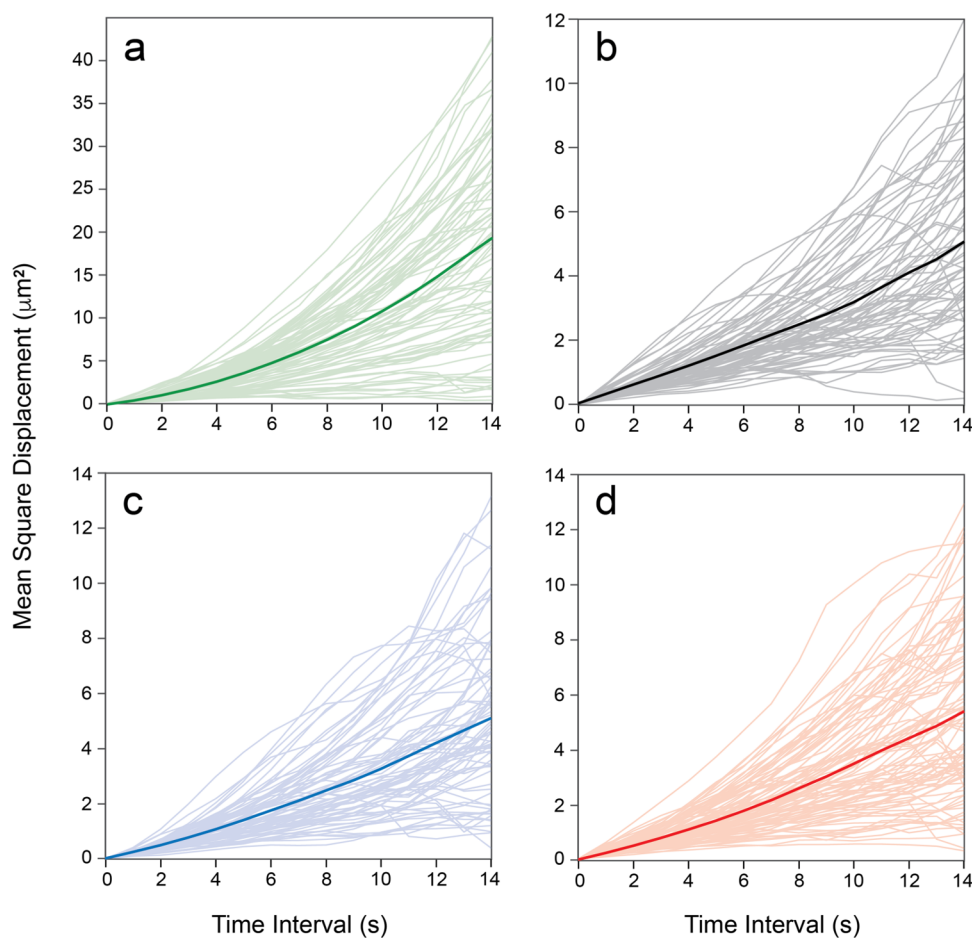


Figure 5. Mean-square displacement (MSD) plots of Janus liposome movement under either enzymatic conversion or control conditions. In each case, the light-color traces in the background represent MSD plots averaged from all particles sampled in individual fluorescence videos, whereas the thick colored line is the ensemble-averaged MSD plot of all particles. (a) MSD plots of HRP- I_4 -attached Janus liposomes in the presence of 1 wt % H_2O_2 . Liposome composition: 35/35/30 DOPC/DPPE/Chol with additional 1% biotin-DOPE; average liposome size: $\sim 4.5 \mu m$, $n = 638$. See also [Video S1](#) for a representative recording of liposome movement. (b) MSD plots of HRP- I_4 -attached Janus liposomes in water alone ($n = 559$; [Video S2](#)). (c) MSD plots of HRP-free Janus liposomes in the presence of 1 wt% H_2O_2 ($n = 494$; [Video S3](#)). (d) MSD plots of HRP-coated homogeneous liposomes in the presence of 1 wt% H_2O_2 . Liposome composition: 70/30 DOPC/Chol with additional 1% biotin-DOPE; $n = 585$ ([Video S4](#)).

extrusion, may as well even out their differences in motion that would otherwise be present.

Comparison of Different Types of Janus Liposome Micromotors. Recently, we reported another liposome motor system based on asymmetrical lipid efflux.³² As Janus liposomes of similar lipid composition and size were employed in both studies, we now move on to a direct comparison of the two in this last section.

Due to the fundamentally different mechanisms involved, several distinctive characteristics can be identified between the two systems: (1) Driving force: The present enzymatic system is based on gas generation/propulsion, whereas the other employs lipid extraction/efflux; (2) Fuel location/availability: The present system uses H_2O_2 as fuel, which is homogeneously present in the system. By contrast, the other system uses cholesterol, which is present only in the liposome bilayer; (3) Active motion direction. In our enzyme-based system, liposomes move predominantly in the I_d -to- I_o direction, whereas the opposite is true for the other system; (4) Identity/impact of effectuator(s). In both cases, the level of fuel present in the system is found to impact liposome active motion directly and significantly. Of the reaction partner to the

fuel, the effect of enzyme loading remains to be explored, whereas the level (but not type) of extracting agents was found to be insignificant in the concentration range tested for the other system; (5) Effect of Janus ratio. While Janus ratio is found to be largely unimpactful here, nearly 1-fold difference in liposome mobility was observed for liposomes of different Janus ratios under lipid extraction conditions.

CONCLUSIONS

We present in this work a new Janus liposome-based micromotor system propelled by regional enzymatic conversion and gas generation. A general strategy for local placement of enzymes is laid out, utilizing domain-specific lipid sorting together with biotin/avidin affinity binding, which can be readily extended to many other water-soluble enzymes to build new liposome micromotors and study other types of asymmetrical lipid-assembled, enzyme-attached colloids. While this work serves to demonstrate the feasibility of such strategy and implementation, further work is clearly needed to address various practical aspects associated with these motors, such as their long-term activity and stability. In relation to our recent work³² on liposome active motion using lipid efflux, moreover,

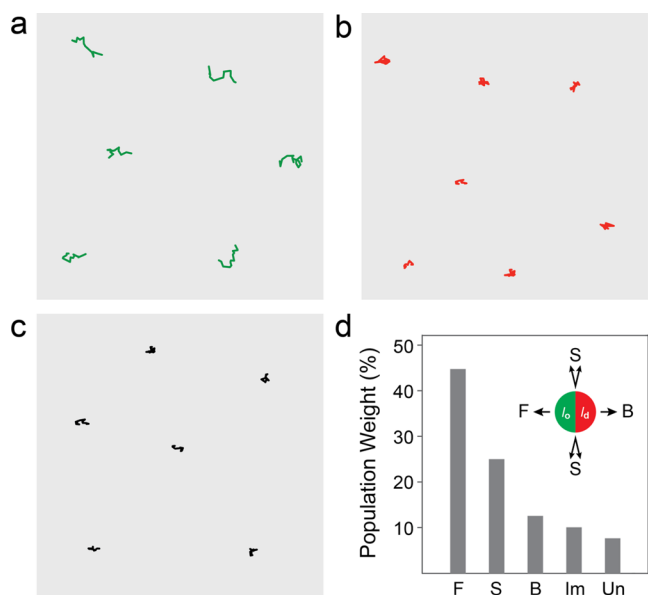


Figure 6. Trajectories of liposome movement under enzymatic conversion conditions and their direction relative to the initial orientation of Janus liposomes. (a) Representative trajectories of HRP-*I_d*-attached Janus liposomes in the presence of 1 wt% H_2O_2 . Liposome composition: 35/35/30 DOPC/DPPC/Chol with additional 1% biotin-DOPE; average liposome size: $\sim 4.5 \mu\text{m}$. (b) Representative trajectories of HRP-free Janus liposomes in the presence of 1 wt% H_2O_2 . (c) Representative trajectories of HRP-attached homogeneous DOPC/Chol liposomes in 1 wt% H_2O_2 . In each case, a gray box of $200 \times 200 \mu\text{m}^2$ is given as size reference. (d) Histogram of trajectory development vs Janus liposome initial orientation of sample in (a): forward (F, with liposome's *I_o* domain as the front), backward (B), sideway (S, which is defined to include trajectories whose initial steps fall within $\sim \pm 15^\circ$ range relative to the phase boundary of a Janus liposome on either side), immobile (Im) and undetermined (Un) particles; $n = 555$.

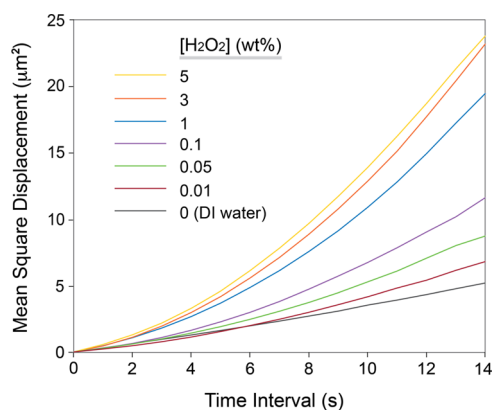


Figure 7. Effect of H_2O_2 concentration on Janus liposome movement under enzymatic conversion conditions. In each case, HRP-*I_d*-attached Janus liposomes consisting of 35:35:30 DOPC/DPPC/Chol and 1% biotin-DOPE were used; average liposome size: $\sim 4.5 \mu\text{m}$. The H_2O_2 concentration was varied from 0 to 5 wt%.

this study stresses once again the importance of particle asymmetry in achieving directional motion and in addition, displays several distinctive features. Sorting out how these features can be controlled and their effects maximized, through fine chemical/structural control of Janus liposomes, is one area on which our ongoing investigation is focused.

EXPERIMENTAL SECTION

Reagents and Materials. All lipids employed in this work, including 1,2-dipalmitoyl-*sn*-glycero-3-phosphocholine (DPPC), 1,2-dioleoyl-*sn*-glycero-3-phosphocholine (DOPC), 1,2-dioleoyl-*sn*-glycero-3-phosphoethanolamine-*N*-(biotinyl) (sodium salt) (biotin-DOPE), 1,2-dioleoyl-*sn*-glycero-3-phosphoethanolamine-*N*-(lissamine rhodamine B sulfonyl) (ammonium salt) (rho-DOPE), and 23-(dipyrometheneboron difluoride)-24-norcholesterol (Bodipy-cho), were products of Avanti Polar Lipids (Alabaster, AL). Other chemicals, including chloroform, poly(vinyl alcohol) (PVA, MW: 145 000), cholesterol, NeutrAvidin, and horseradish peroxidase (HRP) conjugated avidin were obtained from Sigma-Aldrich. Alexa Fluor 488-conjugated avidin was obtained from Thermo Fisher Scientific. Hydrogen peroxide aqueous solutions (30 wt %) were from Macron Fine Chemicals; thermally curable poly(dimethylsiloxane) (PDMS) kits were from Dow Corning Co. Deionized (DI) water of 18.2 M Ω -cm (Millipore) was used throughout this work.

Liposome Preparation. Janus as well as homogeneous liposomes were prepared via gel-assisted hydration as detailed previously.³³ Briefly, dry PVA films were first prepared by spreading drops of a PVA aqueous solution (5 wt%) on precleaned glass slides, followed by drying on a 50 °C hotplate for 0.5 h. On such dry PVA films, lipid stacks were then deposited by spreading small quantities of lipid precursors followed by overnight vacuum drying at room temperature. All lipid precursors used in this work were prepared in chloroform with a total lipid concentration of 5 mM, and for liposome samples intended for motor testing, in addition contain 1 mol % biotin-DOPE. Unless otherwise specified, the lipid precursors also include 0.2 mol % Bodipy-Chol (for the *l_o* phase) and rho-DOPE (*l_d*) each as lipid phase indicators. To yield liposomes, finally, such dried lipid films were hydrated in DI water at 45 °C for either 1 h (biotin-free samples) or 2 h (all samples containing biotin-DOPE). Liposome samples thus prepared appear stable for at least several months (Figure S3) when stored at 4 °C in the dark.

The size-controlled liposomes were prepared by extruding the above-prepared hydration liposome samples one round through a plunger-based lipid extruder (Mini-Extruder, Avanti Polar Lipids) furnished with polycarbonate filter membranes containing track-etched pores of 5- μm nominal diameter (Whatman Nuclepore, GE Healthcare). This extrusion procedure was found to be effective in screening out larger-sized liposomes without significantly disrupting the intended Janus configuration in liposomes (Figure S4). For enzyme-coated liposome samples, this extrusion step was performed after the enzyme/liposome conjugation (see next section). The reported size of these liposomes was determined by the "Analyze Particles" function in ImageJ (version: 2.00-rc-69/1.52n).

Liposome Motor Assembly. Liposome motors were assembled through conjugation between biotin-DOPE-doped liposomes and HRP conjugated with avidin (HRP-avidin). To facilitate binding, a desired volume of HRP-avidin stock solution (0.5 μM in DI water) was pipetted into a 1-mL freshly prepared liposome solution with its effective biotin-DOPE concentration maintained at $\sim 25 \text{ nM}$. Unless otherwise specified, the biotin/avidin binding ratio was kept at 5:1 biotin to HRP-avidin. To facilitate binding, the resulting mixture was first briefly vortexed and then incubated in the dark at 4 °C for 1 h. In the final step, the size of these enzyme-conjugated liposome samples was similarly controlled via one-round extrusion through 5- μm -pore polycarbonate membranes. These avidin-coated liposome samples are found to be stable typically for a week, beyond which significant liposome aggregation becomes evident. To maintain enzyme activity and ensure run-to-run reproducibility, we thus chose to test and monitor the movement of these enzyme-decorated liposome samples typically within the same day of their assembly.

In a related task, another form of avidin, Alexa Fluor 488-labeled avidin, was also employed to fluorescently locate biotin-DOPE in Janus liposomes and determine the optimal avidin/biotin binding ratio in the assembly of liposome motors. To do so, a desired volume of fluorescent-labeled avidin stock solution (0.5 μM in DI water) was pipetted into a 1-mL liposome solution with its final biotin-DOPE

concentration held at ~ 25 nM. The resulting mixture was briefly vortexed and then incubated in the dark at 4°C for 2 h.

Liposome Movement Tracking and Trajectory Analysis.

Fluorescence images of liposomes and video recordings of liposome movement were acquired on a Nikon A1+/MP confocal scanning laser microscope (Nikon Instruments, Melville, NY) using $10\times$ or $20\times$ objectives and excitation laser lines at 488 and 561 nm; the corresponding emission filters are at 525 ± 25 and 595 ± 25 nm, respectively. Using this setup, we monitor liposome movement fluorescently in transparent linear microfluidic channels (dimensions: $200\ \mu\text{m} \times 200\ \mu\text{m} \times 18\ \text{mm}$; product model: thinXXS 100182, Cole-Parmer). Prior to their use, these microchannel slides were thoroughly cleaned by sonication for 30 min each in methanol and then DI water; residual solvents were blow-dried with nitrogen. To start fluorescence recording, dilute liposome samples suspended in either DI water or aqueous H_2O_2 solutions were first pipetted into the microchannels and subsequently sealed off from the surrounding at the two inlets with parafilm to obtain fluid quiescence inside the channel. To avoid channel wall-associated motion complications and ensure run-to-run consistency, only liposomes near the center of microchannels, i.e., $\sim 100\ \mu\text{m}$ away from the channel sides and floor/ceiling, are followed and recorded. Throughout this work, fluorescence videos (in .avi) were recorded at 512×512 pixel resolution at 1 frame/s.

Trajectories of liposomes are obtained by analyzing particle movement fluorescence videos using *TrackMate*, an ImageJ plug-in for single-particle tracking and analysis. The trajectory files (in .xml) thus obtained were then imported into MATLAB to calculate the mean-square displacement (MSD) of particle movement following a published protocol.⁴⁷ To ensure data convergence and obtain robust ensemble-averaged values,^{32,48} we typically analyze >500 liposomes for each sample to obtain the ensemble-averaged MSD plot.

■ ASSOCIATED CONTENT

SI Supporting Information

The Supporting Information is available free of charge at <https://pubs.acs.org/doi/10.1021/acs.langmuir.3c00335>.

Additional experimental details on different biotin/avidin binding ratios and the effect of Janus ratio on liposome motion, liposome stability, and size control (PDF)

Fluorescence video showing movement of HRP- I_{d} -attached Janus liposomes in 1 wt% H_2O_2 (Video S1) (MP4)

Fluorescence video showing movement of HRP- I_{d} -attached Janus liposomes in water alone (Video S2) (MP4)

Fluorescence video showing movement of HRP-free Janus liposomes in 1 wt% H_2O_2 (Video S3) (MP4)

Fluorescence video showing movement of HRP-coated homogeneous liposomes in 1 wt% H_2O_2 (Video S4) (MP4)

■ AUTHOR INFORMATION

Corresponding Author

Wei Zhan – Department of Chemistry and Biochemistry, Auburn University, Auburn, Alabama 36849, United States; orcid.org/0000-0001-7096-9261; Email: wzz0001@auburn.edu

Authors

Hui Jin – Department of Chemistry and Biochemistry, Auburn University, Auburn, Alabama 36849, United States

Jinyan Cui – Department of Chemistry and Biochemistry, Auburn University, Auburn, Alabama 36849, United States

Complete contact information is available at:

<https://pubs.acs.org/10.1021/acs.langmuir.3c00335>

Notes

The authors declare no competing financial interest.

■ ACKNOWLEDGMENTS

This work was supported by the National Science Foundation (Award No. CHE-2108243).

■ REFERENCES

- (1) Sánchez, S.; Soler, L.; Katuri, J. Chemically Powered Micro- and Nanomotors. *Angew. Chem., Int. Ed.* **2015**, *54*, 1414–1444.
- (2) Zhang, J.; Luijten, E.; Grzybowski, B. A.; Granick, S. Active Colloids with Collective Mobility Status and Research Opportunities. *Chem. Soc. Rev.* **2017**, *46*, 5551–5569.
- (3) Wang, L.; Song, S.; van Hest, J.; Abdelsohsen, L. K. E. A.; Huang, X.; Sánchez, S. Biomimicry of Cellular Motility and Communication Based on Synthetic Soft-Architectures. *Small* **2020**, *16*, No. 1907680.
- (4) Ji, F.; Wu, Y.; Pumera, M.; Zhang, L. Collective Behaviors of Active Matter Learning from Natural Taxes Across Scales. *Adv. Mater.* **2022**, *34*, No. 2203959.
- (5) Menger, F. M.; Keiper, J. S. Chemistry and Physics of Giant Vesicle as Biomembrane Models. *Curr. Opin. Chem. Biol.* **1998**, *2*, 726–732.
- (6) Trantidou, T.; Friddin, M.; Elani, Y.; Brooks, N. J.; Law, R. V.; Seddon, J. M.; Ces, O. Engineering Compartmentalized Biomimetic Micro- and Nanocontainers. *ACS Nano* **2017**, *11*, 6549–6565.
- (7) Goldberg, R.; Klein, J. Liposomes as Lubricants: Beyond Drug Delivery. *Chem. Phys. Lipids* **2012**, *165*, 374–381.
- (8) Chang, H.-I.; Yeh, M.-K. Clinical Development of Liposome-Based Drugs: Formulation, Characterization, and Therapeutic Efficacy. *Int. J. Nanomed.* **2012**, *7*, 49–60.
- (9) Shahidi, F.; Han, X.-Q. Encapsulation of Food Ingredients. *Crit. Rev. Food Sci. Nutr.* **1993**, *33*, 501–547.
- (10) Betz, G.; Aeppli, A.; Menshutina, N.; Leunenberger, H. In Vivo Comparison of Various Liposome Formulations for Cosmetic Application. *Int. J. Pharm.* **2005**, *296*, 44–54.
- (11) Rongen, H. A. H.; Bult, A.; van Bennekom, W. P. Liposomes and Immunoassays. *J. Immunol. Methods* **1997**, *204*, 105–133.
- (12) Patiño, T.; Arqué, X.; Mestre, R.; Palacios, L.; Sánchez, S. Fundamental Aspects of Enzyme-Powered Micro- and Nanoswimmers. *Acc. Chem. Res.* **2018**, *51*, 2662–2671.
- (13) Mathesh, M.; Sun, J.; Wilson, D. A. Enzyme Catalysis Powered Micro/Nanomotors for Biomedical Applications. *J. Mater. Chem. B* **2020**, *8*, 7319–7334.
- (14) Safdar, M.; Khan, S. U.; Jänis, J. Progress toward Catalytic Micro- and Nanomotors for Biomedical and Environmental Applications. *Adv. Mater.* **2018**, *30*, No. 1703660.
- (15) Ma, X.; Jannasch, A.; Albrecht, U.-R.; Hahn, K.; Miguel-López, A.; Schäffer, E.; Sánchez, S. Enzyme-Powered Hollow Mesoporous Janus Nanomotors. *Nano Lett.* **2015**, *15*, 7043–7050.
- (16) Dey, K. K.; Zhao, X.; Tansi, B. M.; Méndez-Ortiz, W. J.; Córdova-Figueroa, U. M.; Golestanian, R.; Sen, A. Micromotors Powered by Enzyme Catalysis. *Nano Lett.* **2015**, *15*, 8311–8315.
- (17) Jiang, S.; Chen, Q.; Tripathy, M.; Luijten, E.; Schweizer, K. S.; Granick, S. Janus Particle Synthesis and Assembly. *Adv. Mater.* **2010**, *22*, 1060–1071.
- (18) Loget, G.; Kuhn, A. Bulk Synthesis of Janus Objects and Asymmetric Patchy Particles. *J. Mater. Chem.* **2012**, *22*, 15457–15474.
- (19) Walther, A.; Muller, A. H. E. Janus Particles: Synthesis, Self-Assembly, Physical Properties, and Applications. *Chem. Rev.* **2013**, *113*, 5194–5261.
- (20) Wang, H.; Pumera, M. Fabrication of Micro/Nanoscale Motors. *Chem. Rev.* **2015**, *115*, 8704–8735.
- (21) Zöttl, A.; Stark, H. Emergent Behavior in Active Colloids. *J. Phys.: Condens. Matter* **2016**, *28*, No. 253001.

- (22) Moran, J. L.; Posner, J. D. Phoretic Self-Propulsion. *Annu. Rev. Fluid Mech.* **2017**, *49*, 511–540.
- (23) Patiño, T.; Feiner-Gracia, N.; Arqué, X.; Miguel-López, A.; Jannasch, A.; Stumpp, T.; Schäffer, E.; Albertazzi, L.; Sánchez, S. Influence of Enzyme Quantity and Distribution on the Self-Propulsion of Non-Janus Urease-Powered Micromotors. *J. Am. Chem. Soc.* **2018**, *140*, 7896–7903.
- (24) Szoka, F., Jr.; Papahadjopoulos, D. Comparative Properties and Methods of Preparation of Lipid Vesicles (Liposomes). *Annu. Rev. Biophys. Bioeng.* **1980**, *9*, 467–508.
- (25) Torchilin, V.; Weissig, V. *Liposome: A Practical Approach*; Oxford University Press: Oxford, U.K., 1990.
- (26) Fouladi, F.; Steffen, K. J.; Mallik, S. Enzyme-Responsive Liposomes for the Delivery of Anticancer Drugs. *Bioconjugate Chem.* **2017**, *28*, 857–868.
- (27) Somasundar, A.; Ghosh, S.; Mohajerani, F.; Massenburg, L. N.; Yang, T.; Cremer, P. S.; Velegol, D.; Sen, A. Positive and Negative Chemotaxis of Enzyme-Coated Liposome Motors. *Nat. Nanotechnol.* **2019**, *14*, 1129–1134.
- (28) Ghosh, S.; Mohajerani, F.; Son, S.; Velegol, D.; Butler, P. J.; Sen, A. Motility of Enzyme-Powered Vesicles. *Nano Lett.* **2019**, *19*, 6019–6026.
- (29) Hortelão, A. C.; García-Jimeno, S.; Cano-Sarabia, M.; Patiño, T.; MasPOCH, D.; Sánchez, S. LipoBots: Using Liposomal Vesicles as Protective Shell of Urease-Based Nanomotors. *Adv. Funct. Mater.* **2020**, *30*, No. 2002767.
- (30) Joseph, A.; Contini, C.; Cecchin, D.; Nyberg, S.; Ruiz-Perez, L.; Gaitzsch, J.; Fullstone, G.; Tian, X.; Azizi, J.; Preston, J.; Volpe, G.; Battaglia, G. Chemotactic Synthetic Vesicles: Design and Applications in Blood-Brain Barrier Crossing. *Sci. Adv.* **2017**, *3*, No. e1700362.
- (31) Santiago, I.; Simmel, F. C. Self-Propulsion Strategies for Artificial Cell-Like Compartments. *Nanomaterials* **2019**, *9*, 1680.
- (32) Cui, J.; Jin, H.; Zhan, W. Enzyme-Free Active Liposome Motion via Asymmetrical Lipid Efflux. *Langmuir* **2022**, *38*, 11468–11477.
- (33) Wang, M.; Liu, Z.; Zhan, W. Janus Liposomes: Gel-Assisted Formation and Bioaffinity-Directed Clustering. *Langmuir* **2018**, *34*, 7509–7518.
- (34) Seifert, U. Configurations of Fluid Membranes and Vesicles. *Adv. Phys.* **1997**, *46*, 13–137.
- (35) Israelachvili, J. N. *Intermolecular and Surface Forces*, 3rd ed.; Elsevier Inc.: The Netherlands, 2011; pp 550–558.
- (36) Deserno, M. Fluid Lipid Membranes: From Differential Geometry to Curvature Stresses. *Chem. Phys. Lipids* **2015**, *185*, 11–45.
- (37) The time resolution of our measurements here is limited both instrumentally (1 frame/s recording speed) and by H₂O₂ diffusion. Also see the [Experimental Section](#).
- (38) Orrico, F.; Lopez, A. C.; Saliwonzcyk, D.; Acosta, C.; Rodriguez-Grecco, I.; Mouro-Chanteloup, I.; Ostuni, M. A.; Denicola, A.; Thomson, L.; Möller, M. N. The Permeability of Human Red Blood Cell Membranes to Hydrogen Peroxide Is Independent of Aquaporins. *J. Biol. Chem.* **2022**, *298*, No. 101503.
- (39) Ghysels, A.; Krämer, A.; Venable, R. M.; Teague, W. E.; Lyman, E.; Gawrisch, K.; Pastor, R. W. Permeability of Membranes in the Liquid Ordered and Liquid Disordered Phases. *Nat. Commun.* **2019**, *10*, No. 5616.
- (40) Subczynski, W. K.; Hyde, J. S.; Kusumi, A. Oxygen Permeability of Phosphatidylcholine-Cholesterol Membranes. *Proc. Natl. Acad. Sci. U.S.A.* **1989**, *86*, 4474–4478.
- (41) White, G. F.; Racher, K. I.; Lipski, A.; Hallett, F. R.; Wood, J. M. Physical Properties of Liposomes and Proteoliposomes Prepared from *Escherichia coli* Polar Lipids. *Biochim. Biophys. Acta* **2000**, *1468*, 175–186.
- (42) Motta, I.; Gohlke, A.; Adrien, V.; Li, F.; Gardavot, H.; Rothman, J. E.; Pincet, F. Formation of Giant Unilamellar Proteoliposomes by Osmotic Shock. *Langmuir* **2015**, *31*, 7091–7099.
- (43) Qian, H.; Sheetz, M. P.; Elson, E. L. Single Particle Tracking. Analysis of Diffusion and Flow in Two-Dimensional Systems. *Biophys. J.* **1991**, *60*, 910–921.
- (44) Dunford, H. B.; Stillman, J. S. On the Function and Mechanism of Action of Peroxidases. *Coord. Chem. Rev.* **1976**, *19*, 187–251.
- (45) Hernández-Ruiz, J.; Arnao, M. B.; Hiner, A. N. P.; García-Cánovas, F.; Acosta, M. Catalase-like Activity of Horseradish Peroxidase: Relationship to Enzyme Inactivation by H₂O₂. *Biochem. J.* **2001**, *354*, 107–114.
- (46) Arnao, M. B.; Acosta, M.; del Río, J. A.; Varón, R.; García-Cánovas, F. A Kinetic Study on the Suicide Inactivation of Peroxidase by Hydrogen Peroxide. *Biochim. Biophys. Acta* **1990**, *1041*, 43–47.
- (47) Tinevez, J.-Y.; Perry, N.; Schindelin, J.; Hoopes, G. M.; Reynolds, G. D.; Laplantine, E.; Bednarek, S. Y.; Shorte, S. L.; Eliceiri, K. W. *TrackMate*: An Open and Extensible Platform for Single-Particle Tracking. *Methods* **2017**, *115*, 80–90.
- (48) Novotný, F.; Pumera, M. Nanomotor Tracking Experiments at the Edge of Reproducibility. *Sci. Rep.* **2019**, *9*, No. 13222.